Dhaka Univ. J. Sci. 69(3): 194-201, 2022 (June)
Centennial Special Issue

ISSN 1022 - 2502, E-ISSN 2408-8528
DOI: https://doi.org/10.3329/dujs.v69i3.60030

First-Principles Study of Half Metallic Ferromagnetic and Optical Properties of Nb Doped Cubic ZnS using TB-mBJ Approximation

Md. Borhanul Asfia and Mohammad Abdur Rashid*

Department of Physics, Jashore University of Science and Technology, Jashore 7408, Bangladesh

(Received : 21 November 2021; Accepted : 14 February 2022)

Abstract

Structural, electronic and optical properties of niobium doped ZnS are studied by using full-potential linearized augmented plane wave plus local orbital (FPLAPW+lo) method within the density functional theory (DFT). Computed results of Nb doped ZnS are compared with that of the pristine zinc blende. Tran-Blaha approach of modified Becke and Johnson local spin density approximation (TB-mBJ) is used to study electronic and optical properties. Estimated result shows that Nb reduces the bandgap of ZnS due to hybridization of Nb-4d orbital with S-3p orbital near the Fermi level. Niobium dopant provides half metallic nature to ZnS with 100% spin polarization. Maximum photo-response is noticed in the ultraviolet range for $Zn_{1-x}Nb_xS$ (x = 25, 12.5, 6.25 %). Highest peaks are shifted toward the lower energy range for higher dopant percentage. All these suggest that Nb doped ZnS solid solutions are suitable candidate for both energy filter of UV spectrum and spintronic device.

Keywords: ZnS; DFT method; Electronic band structure; Optical functions; WIEN2k, TB-mBJ.

I. Introduction

Wide bandgap semiconductor materials are important for both scientific and industrial purposes, and they are also used in a number of coating applications because they are less toxic [1]. ZnS is an example of wide bandgap semiconductor and available in two common structures of cubic zinc blende and hexagonal wurtzite with bandgap of 3.82 eV and 3.50 eV respectively [2]. ZnS, because of direct and wide bandgap, can be used for photo-resistor, UV-photo detector, light emitting diode, solar cells and blue lasers [3-6]. Due to sulfur and/or zinc vacancies, ZnS nanocrystals displayed d^0 magnetism. Hence, ZnS nanocrystal is a promising material for applications in spintronic devices. In controlled production of ZnS crystals, defects such as mono or double vacancy with neutral or charged characteristics can be generated. As a result, magnetic and semiconducting properties can be linked in the same material without the need of magnetic atoms, as in Dilute Magnetic Semiconductors (DMSs)[7]. To be commercially visible, a DMS should have a critical temperature (T_c) above room temperature. As a consequence, numerous attempts have been made to elevate T_c above room temperature. In recent years, transition materials (TM) doped ZnS have attracted increasing interest [8]. Different properties, like magnetic, electronic, optical and structural are studied for TM doped ZnS. Room temperature ferromagnetism (FM) and half-metallicity in Fe, Co, Ni, Ti, and V doped ZnS compounds are both confirmed through experimental and theoretical investigations [8-12]. Blue to green photoluminescence is observed for ZnS:Cu nanoparticles [13]. C-doped ZnS is p-type half-metallic ferromagnetic semiconductor and hole mediation is responsible for the ferromagnetism which is confirmed by electronic structures of C-doped ZnS [14]. Experimental results show that thin films of $ZnS_{1-x}Se_x$ solid solutions exhibit a direct bandgap that declines with increasing Se content from 3.50 eV to 2.66 eV, with nonlinear dependence on composition also visible in their bandgap values. Theoretically, it is observed that the lattice parameters of $ZnS_{1-x}Se_x$ vary linearly with the Se composition [15]. The optical bandgap is increased from 3.58 to 3.97 eV with increasing Ni dopant concentrations [10]. Magnetic studies showed, ferromagnetic behavior is increased by Cu doped with ZnS sample which can be described in terms of defect induced ferromagnetism model[16]. The low temperature magnetization measurement for ZnS:Ni confirmed that the DMS have blocking temperature (T_b) well above room temperature and due to magnetic interaction, the nanoparticles are strongly coupled[11]. A ferromagnetic ground state is formed for Ti doped ZnS supercell. The spin polarized Ti atoms arise the magnetic moment in Ti doped ZnS. In addition, Ti separation distance regulates the FM stability of host material, ZnS. FM stability reduces as Ti separation distance grows, indicating that FM coupling between the two doped Ti atoms in the ZnS supercell is short-range [12]. Lower Al concentration regulates the optical bandgap and increases the transmittance coefficient within the visible range of light in ZnS thin films. So ZnS:Al may be a suitable candidate for buffer layer of solar cell [17]. To the best of our knowledge no prior works are reported, either theoretical or experimental, for Nb doped ZnS. In this study, we have investigated the electronic structure and optical properties in Nb doped ZnS by using first-principles calculations. Interestingly, it is found that the considered systems, $Zn_{1-x}Nb_xS$ (x = 0.2500, 0.1250, 0.0625), are half metallic in nature. p-d hybridization in noticed for the band formation of niobium doped ZnS. Promising peak of different optical parameters are noticed in the UV region of the electromagnetic spectrum.

*Author for Correspondence. e-mail: rashid@just.edu.bd

II. Computational Details

The spin polarized full-potential linearized augmented plane wave plus local orbital (FP-LAPW+lo) approach, as incorporated in WIEN2k [18, 19], is used to perform all ab-initio calculations for pristine ZnS and Nb doped ZnS. The FP-LAPW+lo method provides the eigen values and eigen functions of the Kohn-Sham equation [20, 21]. The Perdew-Burke-Ernzerhof generalized gradient approximation (PBE-GGA) [22] is used to construct the exchange-correlation potential in calculating the structural properties. Tran-Blaha approach of the modified Becke-Johnson (TB-mBJ) local spin density approximation [23] is utilized in estimating electronic, magnetic, and optical behaviors. For the base system, ferromagnetic cubic phase of ZnS, which is also known as zinc blend (ZB), is used and the lattice parameters were primarily taken from previously reported work [24]. The FP-LAPW+lo technique assumes a muffin tin model for the crystal potential. The electrons in constituent atoms are separated into two types of states: core and valence. Fully relativistic effects are taken into account in the core states, while scalar relativistic approximation has been used in the valence states. Because the spin orbit effect is so minimal, it is ignored. For core states, a spherical harmonic expansion is used, while for valence states, a plane wave basis set is chosen. The muffin-tin radius (R_{mt}) for Nb, Zn and S were taken to be 2.30, 2.20 and 1.95 a.u. respectively. The plane wave cutoff value was set to $R_{mt} \times K_{max} = 8.5$ for the expansion of the electron wave in the interstitial region. Other parameters that were taken into account in our calculations were: $G_{max} = 12.0$ $(a.u.)^{-1}$, $l_{max} = 10.0$. The self-consistency is established when the differences of total energies in two consecutive cycles is less than 10^{-5} Ry. For the charge convergence the differences were set to be 10^{-4} *e*, where *e* is the electronic charge.

III. Result and Discussion

Structural Properties

In our study we have chosen the most stable cubic structure of ZnS, also known as sphalerite. Zinc blende is a wide bandgap intrinsic semiconductor in which the coordination geometry at Zn and S is tetrahedral. The cubic zinc sulfide crystal belongs to the space group 216 (F-43m) with lattice parameter[9] a = 5.41Å. Zn and S atoms are positioned at (0, 0, 0) and (0.25, 0.25, 0.25) in the crystalline structure, respectively. To generate 25%, 12.5% and 6.25% Nb doped ZnS structures we have generated 1×1×1, 1×2×1 and 2×2×1 super-cell structures respectively from the pristine ZnS structure. Then in each case the Zn atom at (0, 0, 0) is replaced with the niobium atom as shown in Fig1.

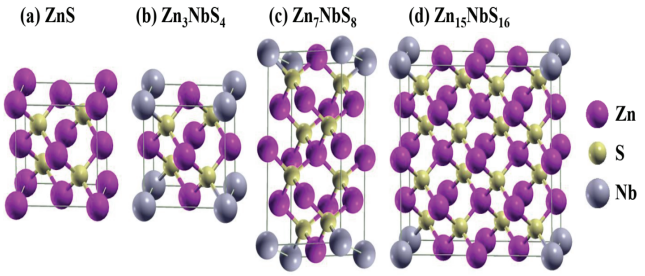

Fig. 1. Crystal structure of (a) pristine ZnS and (b) 25 %, (c) 12.5 %, and (c) 6.25 % niobium doped ZnS.

The total number of atoms in the doped $Zn_{1-x}Nb_xS$ structures were 8, 16 and 32 for $x = 0.25$, 0.125 and 0.0625 respectively. The doped structures are then optimized varying the lattice parameter to find the minimum energy structure. During the optimization and self-consistent field calculation for Zn_3NbS_4 and Zn_7NbS_8 the integration over the Brillouin zone were performed using 1000 *k*-points. However, for $Zn_{15}NbS_{16}$ 2000 *k*-points were used because of the larger size of the unit cell used in simulation. Total energy vs unit cell volume graphs are plotted for each case which are shown in Fig. 2. The computed total energies were fitted to the Birch-Murnaghan equation of state[25] to produce these graphs. In Table 1, the computed equilibrium lattice constant *a*, bulk modulus *B*, and derivatives of the bulk modulus *B'* are listed.

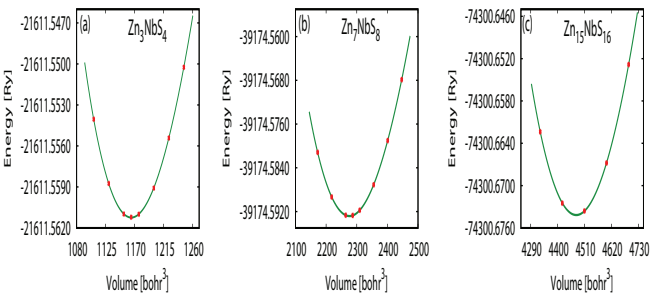

Fig. 2. Spin-polarized total energy versus unit cell volume for of $Zn_{1-x}Nb_xS$ ($x = 0.25$, 0.125, 0.0625).

The value of *a* increases with the increase of Nb concentration in the system due to the larger atomic size of Nb. It is also observed that the value of *B* decreases with increase of dopant concentration.

Electronic band structure

Information about possible energy ranges for electron to occupy/unoccupy an energy state can be furnished from electronic band structure. By taking the differences between valance band maxima and conduction band minima, the electronic bandgap is calculated for both insulator and semiconductor. Band structure of ZnS, 25.0, 12.5 and 6.25 % Nb doped ZnS are calculated by

Table 1. Computed equilibrium lattice constant a, bulk modulus B, and derivatives of the bulk modulus B´ of $Zn_{1-x}Nb_xS$ (x = 25, 12.5, 6.25 %).

Dopant concentration (%)	Lattice constant *a* (Å)	Bulk modulus *B* (GPa)	*B'*
25.0	5.5679	65.0525	5.0698
12.5	5.5242	65.8415	4.7057
6.25	5.4936	67.2433	4.7896

using Tran-Blaha approach of modified Becke and Johnson local spin density approximation, findings are illustrated in **Fig. 3**. From the band structure calculation for cubic ZnS using PBE-GGA approximation, it is found that the bandgap is 2.8 eV [26], which is much lower than the theoretical value 3.7 eV [19,20] and the experimental value 3.74 eV [17]. In this work, TB-mBJ approximation is used and the bandgap is found to be 3.64 eV, which is very close to both experimental and theoretical values for cubic ZnS. That is why Tran-Blaha approach of modified Becke and Johnson local spin density approximation is used in all other calculations to get better result. Interesting properties are noticed when TB-mBJ approximation is used to calculate the band structure. From the band structure of ZnS, it is noticed that the maxima of valance band (VB) and minima of conduction band (CB) are located at Γ point. That mean that ZnS semiconductor have direct bandgap and the value of the bandgap for both spin down and up band is 3.64 eV (Fig. 3(a) and 3(b)). Maxima of VB and the minima of CB are located at point M and Γ respectively for spin up band of 25.0% and 12.5% Nb doped ZnS (Fig. 3(c) and 3(e)). Which indicates that Zn_3NbS_4 and Zn_7NbS_8 has indirect bandgap [27] for up spin. Fig. 3(g) illustrates the spin up band structure of $Zn_{15}NbS_{16}$ where niobium concentration is only 6.25 %. The maxima of VB and the minima of CB are located at point R and Γ respectively giving a indirect bandgap for the up spin of the system. For all considered concentration of the dopant, bandgap vanishes for spin down band and shows metallic nature as demonstrated in Fig. 3(d), 3(f) and 3(h). In all cases the estimated bandgap for spin up structure, whether it is direct or indirect, is in between 0.6 and 0.9 eV. Exact values of spin dependent E_g and the nature of the system are listed in Table 2 as a function of dopant concentration. Nb doped ZnS has a half-metallic nature, with semiconducting up spins and metallic down spins. Half metallic nature is consistent with all considered doping concentration. The computed values of magnetic moment of $Zn_{1-x}Nb_xS$ (x = 0.25, 0.125, 0.0625) are 1.0 (approx.) which demonstrate the ferromagnetic nature of the systems. Table 2 shows the magnetic moments developed in the supercell as a function of niobium concentration.

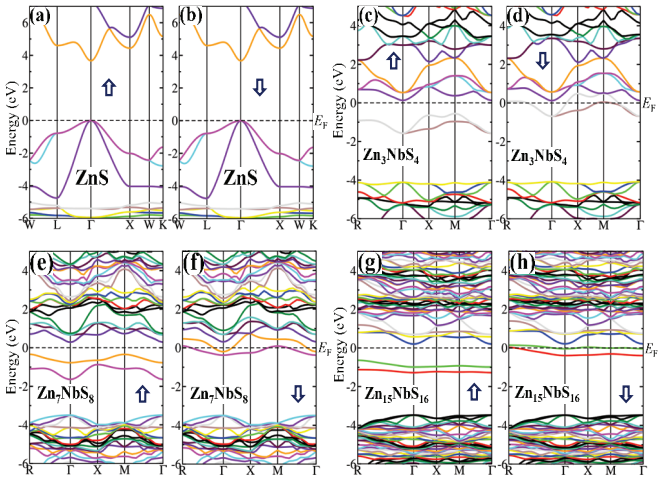

Fig. 3. Electronic Band structure of (a) ZnS spin up, (b) ZnS spin down (c) 25.0 % Nb doped spin up, (d) 25.0 % Nb doped spin down, (e) 12.5 % Nb doped spin up, (f) 12.5 % Nb doped spin down, (g) 6.25 % Nb doped spin up and (h) 6.25 % Nb doped spin down band of ZnS using TB-mBJ approximation.

Table 2. Variation of magnetic moments as a function of niobium doping concentration

Nb doping percentage (%)	System	Bandgap (eV)		Magnetic moment (μ_B)	Nature of the system
		Spin up	Spin down		
0	ZnS (Pristine)	3.640	3.640	0	Semiconductor
25.5	Zn_3NbS_4	0.677	0	1.00019	Half metallic ferromagnet
12.5	Zn_7NbS_8	0.623	0	1.00026	Half metallic ferromagnet
6.25	$Zn_{15}NbS_{16}$	0.837	0	1.00024	Half metallic ferromagnet

Total and projected density of states

Electronic properties of the target material are studied via calculating the density of states (DOS). The contribution of different electronic states in the valance band and conduction band of ZnS, Nb doped ZnS solid solution can determine by using DOS calculation (Fig. 4 and 5). Total DOS calculation as a function of energy for ZnS shows that the DOS of up and down spin are symmetrical, thus there is no indication of spin polarization as shown in Fig. 4 (a). PDOS shows that a strong hybridization of Zn-3d band and S-3p band is taken place for ZnS valance band formation which are presented in Fig. 4 (b, c). Major contribution of S-3p orbital is noticed to form the valance band near the Fermi level. Conduction band of ZnS is contributed by the sulfur 3s and 3p band near the Fermi level. Form Fig. 5(a), (e) and (i), we observe that the TDOS of up and down spins are anti-symmetrical near the fermi level, thus indicates the spin polarization for $Zn_{1-x}Nb_xS$ (x = 0.25, 0.125, 0.0625). When a material exhibits metallic nature in one spin direction and shows an energy bandgap in other spin direction, which offer 100% spin polarization at E_F [28]. In Fig. 5(a), (e) and (i), we also see that $Zn_{1-x}Nb_xS$ (x = 25.0, 12.5, 6.25 %) are metallic in down spin channel and shows energy gap in spin up channel as describe for its band structure calculation. Thus $Zn_{1-x}Nb_xS$ (x = 0.25, 0.125, 0.0625) show half metallic ferromagnetism with 100 % spin polarization as reveled estimated from the band structure calculation. The valance and conduction band mainly composed of Nb-4p, Nb-4d, Zn-3p, Zn-3d and S-3p states for all dopant concentration. Peak of Zn-3d decreases with increasing Nb concentration.

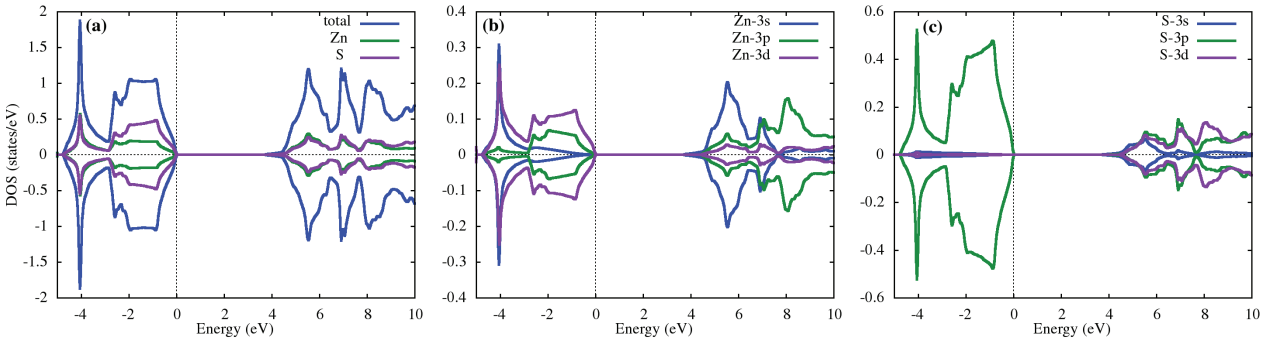

Fig. 4. (a) Density of states of pristine ZnS, projected density of states of significantly contributing orbitals of (b) Zn and (c) S as calculated using TB-mBJ approximation

Optical properties

Optical properties are studied to understand the interactions of photons with Nb doped ZnS. The results are also compared to that of pure ZnS to estimate the changes due to doping. The dielectric function ε(ω) describes the response of a material to the application of an alternating electric field at different photon energy. It has two parts, one is real $\varepsilon_1(\omega)$ and another is imaginary $\varepsilon_2(\omega)$. Real part describes the energy store ability and imaginary part is related to the absorption behavior and electronic band structure of the material [29]. Fig 6(a) represent the imaginary part of dielectric function versus photon energy graph. Peaks are noticed in the figure which indicate the direct transition of electron from valance band to conduction band along the symmetric lines of band structure. The threshold energy is noticed for ZnS and the value is 3.47 eV. This indicates its absorption edge which eventually corresponds to the bandgap of pristine ZnS. Threshold values are absence for $Zn_{1-x}Nb_xS$ (x = 0.25, 0.125, 0.0625) which indicates their half metallic nature as confirmed from their band structure. The maximum computed value of $\varepsilon_2(\omega)$ is shown in the Table 3. Maximum values are in the higher energy range. So, these materials may be used as an energy filter in the UV spectrum.

Change of real part of the dielectric function $\varepsilon_1(\omega)$ with respect to energy spectrum is shown in the Fig. 6(b). Kramer-Kronig (KK) dispersion equation is used to calculate the real part of the dielectric constant [30]. Interestingly, at the zero-energy point 6.25% Nb doped ZnS has zero value of real part of the dielectric function. Negative value is noticed for 12.5 and 25% Nb doped ZnS in the lower photon energy range.

Then $\varepsilon_1(\omega)$ increases with increasing photon energy for all dopant concentration. Peak of $\varepsilon_1(\omega)$ is found in the energy range 4.5 eV to 6.5 eV, where the materials show maximum polarization behavior. Negative value is given when photon energy is further increased above 8.2 eV, 8.26 eV, 8.265 eV and 8.3 eV for ZnS, 6.25%, 12.5% and 25% Nb doped ZnS respectively. In this range material shows metallic nature [31]. A negative peak is noticed for 25% Nb doped ZnS at 6.25 eV. Nb concentration shifts the peak toward lower energy spectrum, which is synchronous to decrease of bandgap.

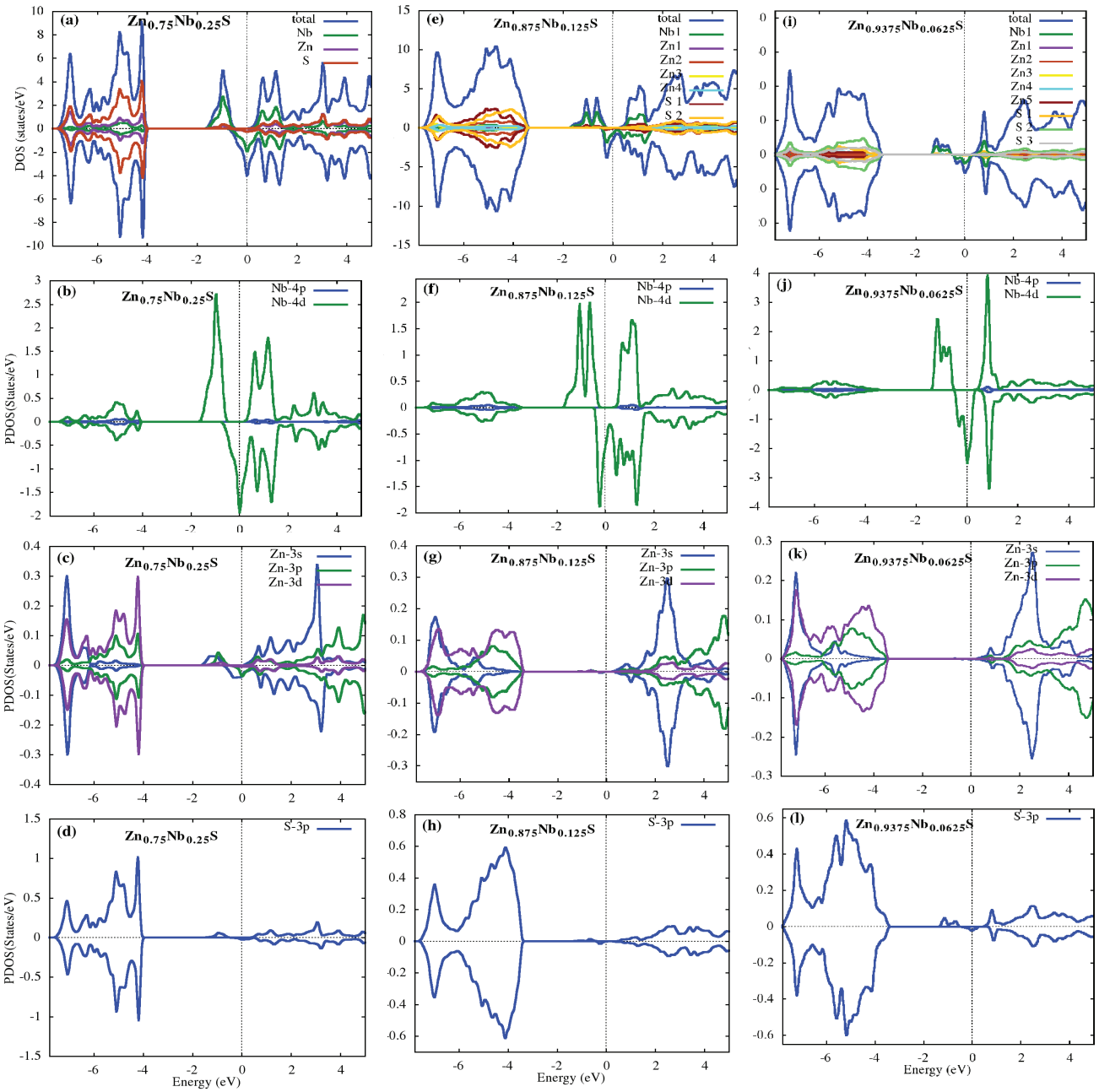

Fig. 5. The total DOS and projected DOS of $Zn_{1-x}Nb_xS$ (x = 0.25, 0.125, 0.0625) as estimated using TB-mBJ approximation. (a), (b), (c) and (d) represents the TDOS and PDOS of atoms and significant contributions of different orbitals when the doping percentage is 25 %. For 12.5% doping concentration these are presented in (e), (f), (g) and (h). In (i), (j), (k) and (l) those values are illustrated for 6.25 % niobium doped ZnS.

Fig. 6(c) represents the variation of refractive index with photon energy. Very high static value of refractive index is notice for 6.25%, 12.5% and 25% Nb doped ZnS. But ZnS has static value of refractive index 2.3. A sharp decrement of refractive index is notice for both 12.5% and 25% Nb doped ZnS in the lower energy range. Refractive index increases within the photon energy range 2.0 eV to 6.3 eV. Maximum peak of the refractive index is noticed in the energy range 4.0 eV to 6.5 eV and listed in the Table 3. With increasing the photon energy above 10 eV, refractive index decreases below unity which indicates that the group velocity of the incident radiation is greater than light velocity

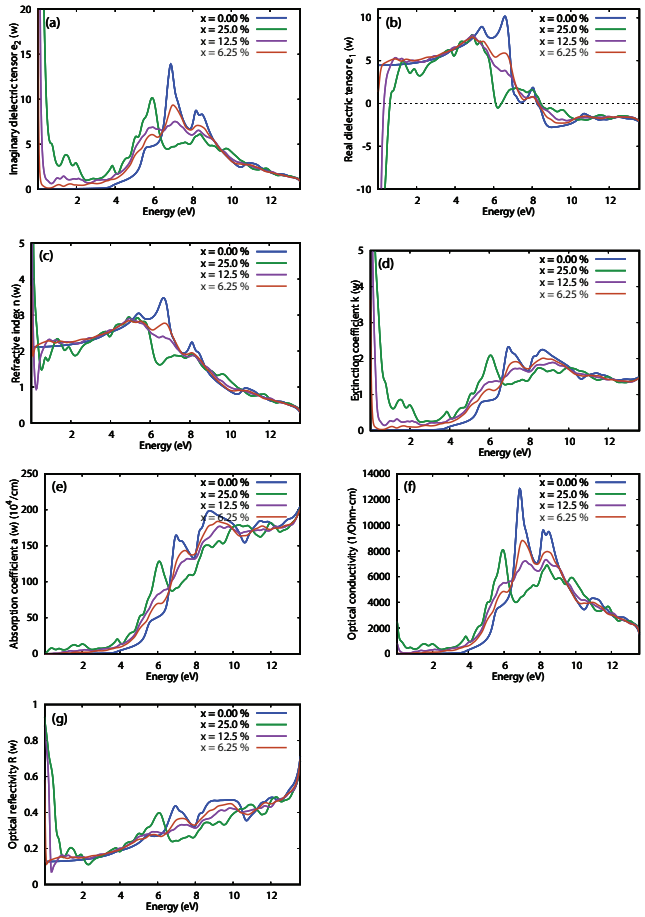

Fig. 6. Optical properties of ZnS, Nb doped ZnS. (a) imaginary and (b) real part of the dielectric constant, (c) refractive index, (d) extinction coefficient, (e) absorption coefficient, (f) optical conductivity and (g) reflectivityas calculated using TB-mBJ approximation

Extinction coefficient (k) and absorption coefficient (α) are related by the relation $k(\omega) = \alpha\lambda/4\pi$, where λ represent the wavelength of light. **Fig. 6(d)** and **6(e)** represent the variation of extinction coefficient and absorption coefficient with photon energy respectively. In the lower energy range, high value of extinction coefficient is noticed but their absorption coefficient is very low for 6.25%, 12.5% and 25% Nb doped ZnS, which indicate their metallic nature. Interestingly, their extinction coefficient decreases sharply up to 2 eV and shows nearly similar nature. Extinction and absorption coefficient is increasing for further increment of photons energy. Maximum value for extinction coefficient is noticed in the energy 6.0 eV to 9.0 eV and it is also listed in **Table 3**. The critical point of the absorption spectra is 3.7 eV for ZnS. Critical points for 6.25%, 12.5% and 25% Nb doped ZnS are noticed at the origin due to their metallic nature. Increasing behavior of absorption is notice for all concentration of Nb in the energy range 2.0 eV to 13.0 eV and a few oscillations are also obtained within 6.0 eV to 12.0 eV photon energy range.

Optical conductivity of a material is very important for optoelectronic application. **Fig. 6(f)** shows the changes of optical conductivity with photon energy. Starting point for ZnS optical conductivity is 3.8 eV. When 6.25% Nb is doped with ZnS, it is sifted to 0 eV and starting points for both 12.5% and 25% are absent in the figure. Maximum value of the optical conductivity is noticed in the energy 6.0 eV to 8.5 eV and specified in the **Table 3**. Variation of the reflectivity of ZnS and Nb doped ZnS are shown in the **Fig. 6(g)**. Static value of the reflectivity for ZnS and 6.25%, 12.5%, 25% Nb doped ZnS is 0.12, 0.63, 0.88 and 0.92 respectively. Reflectivity increases with increasing photon energy and oscillation is noticed in the energy range 6.0 eV to 12.0 eV.

Table 3. Estimated refractive index $n(0)$, maximum value of $\varepsilon_1(\omega)$ and $\varepsilon_2(\omega)$, minimum negative value of $\varepsilon_1(\omega)$, maximum value of $n(\omega)$, absorption edge of extinction coefficient $k(\omega)$ and maximum peak of optical conductivity σ(ω) for Nb doped ZnS.

Parameter	Doping percentage (%) of Nb in ZnS compared to Zn			
	0	25.0	12.5	6.25
$\varepsilon_2(\omega)_{max}$	14	10	7.1	8.9
$\varepsilon_1(\omega)_{max}$	10.2	7.6	6.8	7.5
$\varepsilon_1(\omega)_{min}$	-3	-2.4	-2.3	-2.5
$n(0)$	2.3	6.0	6.0	2.4
$n(\omega)_{max}$	3.6	2.9	2.7	2.8
$k(\omega)_{max}$	2.4	2.2	1.9	2.0
$\sigma(\omega)_{max}$	13000	8200	7500	8700

IV. Conclusions

Based on the first-principles calculations in WIEN2k package, we found that ZnS has wide direct bandgap of 3.64eV. Nb doped ZnS has indirect bandgap in spin up band and absence of bandgap in spin down band which indicates the half metallic nature of Nb doped ZnS. Computed values of the bandgap of 6.25%, 12.5% and 25% Nb doped ZnS are 0.837 eV, 0.623 eV and 0.677 eV in spin down band. Valance band of ZnS near the Fermi level is mainly composed of Zn-3p, Zn-3d and S-3p orbital. Composition of Zn-3s, Zn-3p, S-3p and S-3d orbital is formed the conduction band of ZnS is near the Fermi level. For the Nb doped ZnS, valance band is formed by the composition of Nb-4d, S-3p and conduction band is composed by Nb-4d, Zn-3s and Zn-3p near the Fermi level. The peaks of different optical parameters are noticeable in the UV region of the electromagnetic region. Peaks are shifted toward the lower energy range with increasing the dopant percentage. These Computed results suggest that Nb doped ZnS solid solutions can be a promising candidate for both spintronic device and energy filter of UV spectrum.

Acknowledgement

Mohammad Abdur Rashid would like to thank Prof. Peter Balah, TU, Vienna for providing WIEN2k code.

Credit authorship statement

Md. Borhanul Asfia: Formal analysis, writing original draft, review-editing; **Mohammad Abdur Rashid**: Formal analysis, conceptualization, calculation, supervision, validation, writing original draft, review-editing.

Declaration of competing interest

There is no conflict of interest to declare.

Data availability

The datasets generated and/or analyzed in this study are available from the corresponding author upon reasonable request.

References

1. Stella, R. J., G. T. Rao, V. P. Manjari, B. Babu, C. R. Krishna, R. V. S. N. Ravikumar, 2015 Structural and optical properties of CdO/ZnS core/shell nanocomposites, J. Alloy. Comp. 628 39-45, https://doi.org/10.1016/j.jallcom.2014.11.201
2. Long, D., M. Li, D. Meng, Y. He, 2018 Electronic-structure and thermodynamic properties of $ZnS_{1-x}Se_x$ ternary alloys from the first-principles calculations, Comp. Mater. Sci. 149 386-396, https://doi.org/10.1016/j.commatsci.2018.03.046
3. Patil, D., D. Gautam, 2004 Analysis of effect of temperature on ZnSSe based blue laser diode characteristics at 507 nm wavelength, Phys. B 344 140–146, https://doi.org/10.1016/j.physb.2003.09.249
4. Nasrallah, S. A. B., S. B. Afia, H. Belmabrouk, M. Said, 2005 Optoelectronic properties of zinc blende ZnSSe and ZnBeTe alloys, Eur. Phys. J. B 43 3–9, https://doi.org/10.1140/epjb/e2005-00021-y
5. Ichimura, Y., K. Kishino, M. Satake, M. Kuramoto, A. Yoshida, 1995 Characterization of N-doped MgZnSSe compound system grown on intentionally misoriented GaAs substrates by molecular beam epitaxy, J. Cryst. Growth 150 812–816, https://doi.org/10.1016/0022-0248(95)80052-E
6. Okuyama, H., E. Kato, S. Itoh, N. Nakayama, T. Ohata, A. Ishibashi, 1995 Operation and dynamics of ZnSe/ZnMgSSe double heterostructure blue laser diode at room temperature, Appl. Phys. Lett. 66 656–658, https://doi.org/10.1063/1.114120
7. Faita, F. L., K. Ersching, C. M. Poffo, L. C. Benetti, D. M. Trichês, S.M. Souza, A. D. C. Viegas, J. C. Lima, 2014 Structural, thermal, magnetic and optical characterization of undoped nanocrystalline ZnS prepared by solid state reaction, J. Alloy. Comp. 590 176–183, http://dx.doi.org/10.1016/j.jallcom.2013.12.094
8. Chen, H. X., 2012 First-principle study on magnetic properties of Mn/Fe codoped ZnS, J. Magn. Magn. Mater. 13 2086–2090, https://doi.org/10.1016/j.jmmm.2012.02.011
9. Rabbani, S. F., I. B. S. Banu, 2017 An ab-initio calculation of half-metallic ferromagnetism in vanadium doped ZnS, J. Alloy. Comp. 695 3131-3138, http://dx.doi.org/10.1016/j.jallcom.2016.11.336
10. Jothibasa, M., C. Manoharanb, S. J. Jeyakumara, P. Praveenc, I. K. Punithavathya, J. P. Richarda, 2018 Synthesis and enhanced photocatalytic property of Ni doped ZnS nanoparticles, S. Energy 159 434–443, https://doi.org/10.1016/j.solener.2017.10.055
11. Patel, P. C., S. Ghosh, P. C. Srivastava, 2018 Bound magnetic polaron driven room-temperature ferromagnetism in Ni doped ZnS nanoparticles, M. Chem. Phy. 216 285–29, https://doi.org/10.1016/j.matchemphys.2018.05.065
12. Chen, Y. W. Mi, J. Yang, Q. Song, H. Yan, T. Wei, Y. Guo, 2015 Electronic structures and magnetic properties in Ti-doped ZnS, S. S. Comm. 205 9–13, http://dx.doi.org/10.1016/j.ssc.2014.12.018
13. Klausch, A. H. Althues, C. Schrage, P. Simon, A. Szatkowski, M. Bredol, D. Adame, S. Kaske, 2010 Preparation of luminescent ZnS:Cu nanoparticles for the functionalization of transparent acrylate polymers, J. Lumin. 130 692–697, http://dx.doi:10.1016/j.jlumin.2009.11.021
14. Chen, H.X. 2011 First-principles study on the magnetic property of C-doped wurtzite ZnS, P. Letters A 375 2444–2447, http://dx.doi:10.1016/j.physleta.2011.05.013
15. Hussaina, S. L. Guoa, H. Louisa, S. Zhua, T Hea, 2019 First-principles calculations of wurtzite ZnS1-xSex solid solutions for Photocatalysis, M. T. Com. 21 100672, https://doi.org/10.1016/j.mtcomm.2019.100672
16. Patel, P. C. S. Ghosh, P. C. Srivastava, 2017 Effect of impurity concentration on optical and magnetic properties in ZnS:Cu nanoparticles, P. E 93 148–152, http://dx.doi.org/10.1016/j.physe.2017.06.009
17 Maria, K. P. Sultana, M. B. Asfia, 2020 Chemical bath deposition of aluminum doped zinc sulfide thin films using non-toxic complexing agent: Effect of aluminum doping on optical and electrical properties, A. Adv. 10 065315; http://dx.doi:10.1063/5.0011191
18 Blaha, P. K. Schwarz, G. Madsen, D. Kvasnicka, J. Luitz, R. Laskowsk, F. Tran, L. Marks, L. Marks, 2019 WIEN2k: An Augmented Plane Wave Plus Local Orbitals Program for Calculating Crystal Properties, Techn. Universitat, .
19. Blaha, P. K. Schwarz, F. Tran, R. Laskowski, G. K. H. Madsen, L. D. Marks, 2020 WIEN2k: An APW+lo program for calculating the properties of solids, J. Chem. Phys. 152 074101, https://doi/10.1063/1.5143061
20. Hohenberg and W. Kohn, 1964 P. Inhomogeneous electron gas, P. Review 136 864-71, https://doi.org/10.1103/PhysRev.136.B864
21. Kohn, W. L. J. Sham, 1965 Self-Consistent Equations Including Exchange and Correlation Effects, 140 1113, https://10.1103/PhysRev.140.A1133

22. Perdew, J. P. K. Burke, M. Ernzerhof, 1997 Generalized Gradient Approximation Made Simple, Phys. Rev. Lett. 78 1396. https://journals.aps.org/prl/abstract/10.1103/PhysRevLett.77.3865

23. Tran, F. P. Blaha, 2009 Accurate Bandgaps of Semiconductors and Insulators with a Semilocal Exchange-Correlation, Potential, Phys. Rev. Lett. 102 226401 https://journals.aps.org/prl/abstract/10.1103/PhysRevLett.102.226401

24. Murnaghan, F. D. 1944 The Compressibility of Media under Extreme Pressures, 15 244-247, https://doi.org/10.1073/pnas.30.9.244

25. Mahmood, Q. G. Murtaza, R. Ahmed, T. Hussain, I.G. Will, 2016 First principle study of vanadium doped ZnS: Structural, electronic, elastic, magnetic and optical properties using mBJ approximation, Curr. Appl. Phys. 3 361-370, https://doi.org/10.1016/j.cap.2015.12.024

26. Monir, M. E. A. H. Baltache, R. Khenata, G. Murtaza, R. A. Waleed, K. Ahmed, S. B. Omran, A. Bouhemadou, 2016 Half-metallicity and optoelectronic properties of V-doped zincblende ZnS and CdS alloys, Inter. J. Mod. Phys. B 30 1650034, https://doi.org/10.1142/S021797921650034X

27 Nazir, S. N. Ikram, S. Siddiqi, Y. Saeed, A. Shaukat, A. H. Reshak, 2010 First principles density functional calculations of half-metallic ferromagnetism in $Zn_{1-x}Cr_xS$ and $Cd_{1-x}Cr_xS$, Curr. Opin. Solid State Mater. Sci. 14 1-6, https://doi.org/10.1016/j.cossms.2009.08.001

28 Birch, F. 1947 Finite elastic strain of cubic crystal, phys. Rev., 71 809.

29 Hussain, S. G. Murtaza, S. H. Khan, A. Khan, M. A. Ali, M. Faizan, A. Mahmood, R. Khenata, 2016 First principles study of structural, optoelectronic and thermoelectric properties of Cu2CdSnX4 (X= S, Se, Te) chalcogenides, Mater. Res. Bull. 79 73–83, https://doi.org/10.1016/j.materresbull.2016.03.001

30. Zahedi, E. M. Hojamberdiev, M. F. Bekheet, Lectronic, 2015 optical and photocatalytic properties of three-layer perovskite Dion–Jacobson phase CsBa2M3O10 (M = Ta, Nb): a DFT study, RSC Adv. 5 88725–88735, https://doi.org/10.1039/C5RA13763B

31. Sun, B. Xu, X. Li, J. L. Yi, 2008 Electronic structure, ferroelectricity and optical properties of $CaBi_2Ta_2O_9$, Eur. Phys. J. B 66 483–487, https://doi.org/10.1140/epjb/e2008-00461-9